NUMERICAL STUDY OF FLOW BOILING IN INCLINED LARGE LENGTH-DIAMETER MICROCHANNELS

Xinyu He[a1], Dechang Wang[a1]*, Qinglu Song[a2]*, Zhanjie Liu[b3]*, Sai Zhou[a3]*

[a]College of Mechanical and Electrical Engineering, Qingdao University, Qingdao, China

[b]Haier Biomedical Co. Ltd, Qingdao, China

1.* Corresponding author: wdechang@163.com

2.* Corresponding author: sql@qdu.edu.cn

3.* Corresponding author: liuzj@haier.com

The present study aims to numerically investigate the impact of inclination angle on the boiling heat transfer and pressure drop in rectangular microchannel tubes with a large length-diameter ratio. The volume of fluid approach was utilized to model the two-phase flow in microchannels using the computational fluid dynamics method. The effects of different inclination angles, aspect ratio and Reynolds number on heat transfer and pressure drop characteristics are analyzed by simulation. According to the latent heat percentage and saturation temperature differential, the mass transfer factor was calculated using the Lee model, which describes the mass and energy transfer throughout the boiling process. The convective heat transfer coefficients of the walls of structures at angles ranging from 0° to 90° (aspect ratios of 1.271, 1.017 and 0.763, respectively) were analyzed. It was found that with the decrease of aspect ratios, the convective heat transfer coefficients decreased by 16.64% and 11.56%, respectively. In order to keep the evaporator outlet superheat within 5 °C, the inlet Reynolds number should not be lower than 3000. The study offers insightful information for designing and refining microchannel evaporators in refrigeration systems, particularly for horizontal freezers with specific inclination angle arrangements.

Keywords: *large length-diameter ratio, inclination angle, aspect ratio, low-mass flow rate, CFD simulation, flow boiling heat transfer*

1. Introduction

To optimize the operation of refrigeration systems utilizing environmentally friendly refrigerants, it is important to review the individual components. Evaporator as the basic equipment of refrigeration and air conditioning system, its size should be appropriate. Microchannel tube has good heat dissipation performance and has broad application prospect in high power density thermal elements [1-4]. Aluminum microchannel tubes have attracted great attention due to their lower cost and high thermal system compatibility compared to copper. In a microchannel evaporator, the refrigerant evaporates by removing heat from the space or object being cooled. Microchannel flow boiling involves complex phase change dynamics and flow instabilities, necessitating advanced experimental and computational study. In addition, the current research on microchannel heat exchange tubes is mainly aimed at the heat dissipation of high-power components. Numerous sophisticated engineered surfaces or micro/nanostructured microchannels have been created to greatly increase the rates of heat transmission in single phases and flow-boiling. Surface modifications and geometric designs of tube, including

triangular cavities [5,6], microneedle and micro-pin fin arrays [7-9], staggered herringbone microchannels [10], cavity-rib pairs [11], and countercurrent microchannels [12] have been intensively researched to optimize thermal performance in single-phase and flow boiling scenarios.

However, in the refrigeration system of the chest freezer, the choice of the evaporator structure is still restricted by the system cooling capacity, the pressure difference that the compressor can handle, and the thermal uniformity in the chassis. To improve heat sinks' ability to transport heat in small areas, Hung et al. adopted a double-layer structure [13] and utilized fluorinated nanofluids [14,15] for experimentation, which offers important reference value for the creation of cooling systems that are more dependable and efficient.

In the microscale constrained environment, laminar flow is quite prevalent because of the chest freezer's modest refrigerant charge quantity [16,17]. It is also common to choose complex microchannel structures to significantly increase the boiling heat transfer rate of two-phase flow. [18-21]. However, due to the factors such as pressure drop, thermal uniformity and economy, the complex micro-channel structure cannot be directly applied to the low charge refrigeration system to increase the heat transfer rate at boiling in a two-phase flow. At present, the flow-boiling heat transfer process's design in chest freezer refrigeration system mainly relies on empirical data. Consequently, the numerical simulation of porous microchannel flat tubes with large length-diameter and different aspect ratios is very important to guide experimental research and system development. Numerical simulations using the Volume of Fluid (VOF) method are suitable for simulating two-phase flows [22-24].

In the simulation process of the evaporator of the chest refrigerator, it is necessary to choose the appropriate analysis method based on the evaporator heat exchange tube's inclination angle, the refrigerant flowrate and quality of vapor at the inlet, the import and export temperature, and the heat transfer of the heat exchange tube to the inner wall, so as to complete the physical modeling and the setting of the boundary conditions. At present, the numerical research on the boiling heat transfer of enhanced microchannel heat exchangers mainly focusing on modifying the geometry of the heat exchange tube, adjusting the boundary conditions and improving the parameters of the mathematical model. Liu et al. [25,26] took the evaporator inclination angle as the starting point to analyze the changing trend of evaporator pressure drop under different inclination angles. In the simulation, emphasis was placed on the interaction between gravity field and velocity field in the tube.

The heat and mass transport capabilities of microchannel tubes with a 1.0 mm inner diameter were examined by Saisorn et al. [27] and Oliveira et al. [28]. Variations in inclination angle and two-phase flow pattern were examined using pressure drop and two-phase flow pattern as the study objects. Hajar and Teng [29] studied the significant correlation between the inclination angle and the heat transfer coefficient at a fixed angle in the study of gravity heat pipe. In the flow boiling process, the influence of inclination on heat transfer cannot be ignored, especially in the harsh operating conditions of heat pump water heaters, solar collectors, horizontal freezers and other compact heat transfer devices. They have specific incline arrangements and resistance requirements.

For decades, significant scholarly attention has been directed toward examining the effects of the length-diameter (L/D_h) ratio on flow boiling performance. Studies on critical heat fluxes (CHFs) in microchannel flow boiling, both theoretical and experimental, have shown that high L/D_h ratios considerably impair ideal flow boiling behavior [30–32]. This is primarily attributed to the challenges associated with eliminating confined bubbles and ensuring adequate liquid supply to the outlet region. In addition, a large L/D_h ratio negatively impacts the flow of two-phase transport. The function of hydraulic diameter fluctuations was further examined by Wang et al. [33]. Their findings demonstrated that large L/D_h ratios frequently limit rapid liquid transfer to the channel exit. Therefore, early drying out is associated with the early development of CHF. For effective boiling heat transfer to continue, liquid rewetting and worldwide liquid transport are necessary. However, most of the present investigations on L/D_h were restricted to the impact of L/D_h on flow boiling performance and the enhancement mechanism of L/D_h on the microchannel flow heat transfer. Considering the actual engineering scenario, it is still important to analyze the large L/D_h microchannel heat exchanger for the flow heat transfer in the cold cabinet refrigeration system.

In addition, Lee model was usually used for numerical simulation of fluid boiling heat transfer and flow [34], in which mass transfer factor had a great influence on gas-liquid interface tracking [35-38]. In the existing studies, the mass transfer factor of Lee model was mostly fixed value [39-45]. But in fact, when the mass transfer factor was fixed under various working conditions, the simulation results

would deviate significantly from the actual conditions [46]. Qiu et al. [47] proposed a method to determine the mass transfer factor in Lee's phase-change mass transfer equation. They introduced two evaluation indexes (latent heat share and saturation temperature difference) to assess the rationality of the mass transfer factor. By deriving theoretical expressions for these indexes, they analyzed how the factor impacts simulation results. Their analysis explains the wide range of values reported in literature and offers practical guidelines for selecting the mass transfer factor. Optimizing the mass transfer factor in model selection significantly boosts the fidelity of the calculations. The less the convergence, the longer the calculation takes. Therefore, the value of the mass transfer factor in the phase transition model was crucial for reducing the computation time, enhancing accuracy, and ensuring better convergence across varying geometric conditions and flow-boiling states.

In this study, derived from the theoretical relations of latent heat distribution and saturation temperature variation, a simulation model was established to simulate the two-phase flow boiling in a rectangular microchannel with large L/D_h ratio, variable inclination angles and variable aspect ratio. The influence of the mass transfer factor on the simulation results was analyzed, and the correctness of the simulation model was verified by the experimental data obtained under certain conditions. After the mass transfer factor has been determined, numerical simulation was used to examine the impacts of flow boiling heat transfer and pressure drop in the rectangular microchannel structure (large L/D_h ratio) of the horizontal freezer refrigeration system with varying inclination angles, aspect ratios and *Re*. The results of this study will be of great significance for determining the winding inclination angle of micro-channel heat exchange tubes when they are applied to the evaporators of refrigerators and chest freezers. The established numerical simulation method can be extended to other two-phase flow systems, and the parametric study framework is applicable to various refrigerants.

2. Physical and Numerical Models

2.1. Computational domain

The variation of inclination angles, which critically impacts the flow and thermal transfer characteristics of the microchannel evaporator, is illustrated in Fig. 1. Fig. 2 shows the microchannel structure's precise geometric properties, such as the channel's width, height, and length. The thermophysical properties of R600a dynamic viscosity μ (kg/(m·s)), specific heat capacity *Cp*(J/(kg·°C)), and density ρ(kg/m^3)) were determined using REFPROP between -48°C and 50°C, covering the operational limits of the evaporator. A segmented linear interpolation function was employed in the FLUENT solver to ensure accurate property assignment and to model the flow boiling behavior effectively.

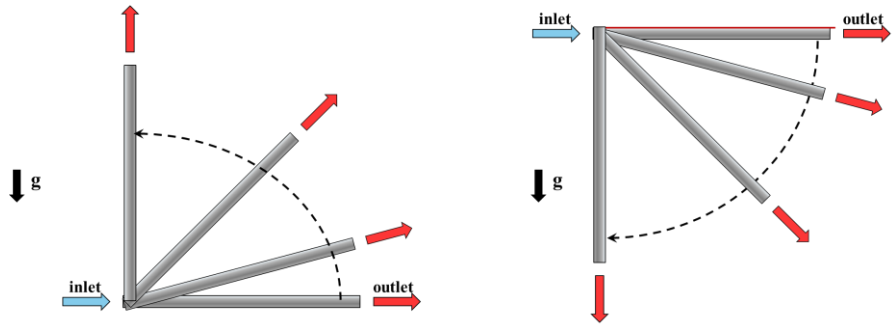

(a) φ=0°-90° (b) φ=0°-(-90°)

Fig. 1. Inclination angle configurations of evaporator orientations (±0°–90°)

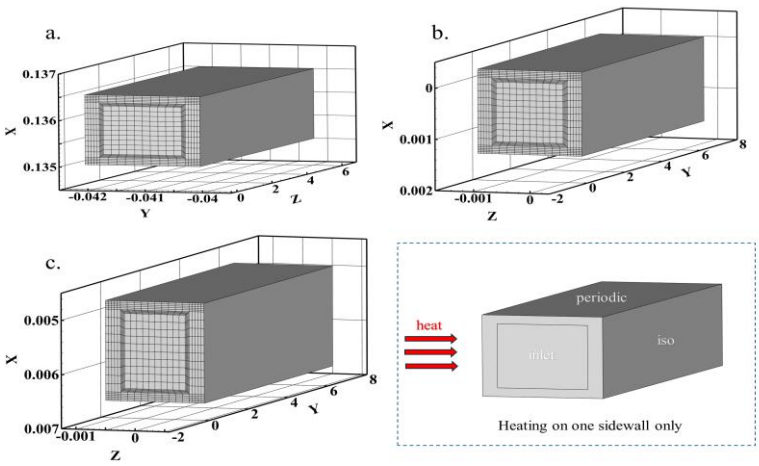

Fig. 2. Microchannel geometries and boundary conditions for different β: (a) β=1.271 (b) β=1.017 (c) β=0.763.

2.2. Mathematical model

2.2.1 VOF model

The Volume of Fluid (VOF) model is a widely adopted interface-capturing technique designed to track the interfaces between multiple immiscible fluids. In this approach, because the momentum equations are the same for all fluid phases, the computational domain allows for the tracking and resolution of the volume fraction of each phase. The volume fractions of the liquid and gas phases' continuity equations are solved in order to accomplish the dynamic development of the interface [48]. The momentum equation, energy equation, and continuity equations are all included in the governing equations and have the following expression.

(1) Continuity equation:

$$\frac{\partial}{\partial t}\left(\alpha_l \rho_l\right)+\nabla\cdot\left(\alpha_l \rho_l v\right)=S_l \tag{1}$$

$$\frac{\partial}{\partial t}\left(\alpha_v \rho_v\right)+\nabla\cdot\left(\alpha_v \rho_v v\right)=S_v \tag{2}$$

(2) Momentum equation:

$$\frac{\partial}{\partial t}\left(\rho v\right)+\nabla\cdot\left(\rho v v\right)=-\nabla P+\nabla\cdot\left[\mu\left(\nabla v+\nabla v^{\mathrm{T}}\right)\right]+\rho \mathrm{g}+\mathrm{F} \tag{3}$$

$$\rho=\alpha_l \rho_l+\alpha_v \rho_v \tag{4}$$

$$\mu=\alpha_l \mu_l+\alpha_v \mu_v \tag{8}$$

(3) Energy equation:

$$\frac{\partial}{\partial t}\left(\rho E\right)+\nabla\cdot\left[v\left(\rho E+P\right)\right]=\nabla\cdot\left(k\nabla T\right)+S_e \tag{6}$$

$$E=\frac{\alpha_l \rho_l E_l+\alpha_v \rho_v E_v}{\alpha_l \rho_l+\alpha_v \rho_v} \tag{7}$$

where S (kg/s) is the rate of mass transfer per volume unit, v (m/s) is the velocity. g (m/s^2) is the acceleration of gravity, F (kg·m/s^2) is the external force, t (s) is the time, P (kg/m^2) is the pressure, T (°C) is the temperature, E (J) is the energy, and S_e (W/m^3) is the energy source term. The density ρ (kg/m^3), dynamic viscosity μ (kg/(m·s)), and thermal conductivity k (W/(m·°C)) represent the properties of the mixed phase, respectively. The liquid and gas phases are denoted by the subscripts l and v, respectively.

2.2.2 Phase transition model

The fluid flow in the tube is always in a turbulent state during the phase change heat transfer process. The following presumptions were made to optimize the model and simulation [49].

(1) The fluid is Newtonian and incompressible.

(2) The thermo-physical properties of the working fluid are temperature-dependent.

(3) Radiative heat transfer is neglected.

(4) Gravitational effects are considered.

(5) The velocity profile at the channel inlet is assumed to be uniform.

The trial calculation stage relies on simplified assumptions and methods to rapidly assess system performance. The difference in inlet and outlet pressure and temperature is less affected by the inclination angle during the trial calculation stage. To enhance the accuracy of the numerical simulation of refrigerant flow boiling in microchannels, the dependence of saturation temperature on pressure was explicitly incorporated, building upon the foundation established in previous studies [50]. The saturation temperature was derived from the saturation pressure using a piecewise linear fitting method. Once the temperature of the liquid exceeds the corresponding saturation temperature (T_{sat} = -25 °C) [51], bubble nucleation initiates. To model the mass and energy transfer during the boiling process, the Lee model [52] was employed, which assumes that the phase transition occurs under thermal equilibrium conditions.

Source term of mass:

$$\begin{aligned} S_{\mathrm{M}} &= -r_{\mathrm{l}}\alpha_{\mathrm{l}}\alpha_{\mathrm{l}}\frac{T_{\mathrm{l}}-T_{\mathrm{sat}}}{T_{\mathrm{sat}}} \qquad T \geq T_{\mathrm{sat}} \\ S_{\mathrm{M}} &= r_{\mathrm{v}}\alpha_{\mathrm{v}}\alpha_{\mathrm{v}}\frac{T_{\mathrm{v}}-T_{\mathrm{sat}}}{T_{\mathrm{sat}}} \qquad T < T_{\mathrm{sat}} \end{aligned} \tag{8}$$

Source term of energy:

$$S_{\mathrm{E}} = -S_{\mathrm{M}}h_{\mathrm{fg}} \tag{9}$$

In this context, α denotes the volume fraction, ρ is the density, h_{fg} represents the latent heat of vaporization, r corresponds to the time of relaxation, and the subscripts l and v refer to the liquid and vapor phases, respectively.

For the mass transfer factor (r), a high value of r guarantees that the simulated results are universally applicable and, in any event, closely resemble the real outcomes. However, excessive r-value leads to non-convergence of the energy equation in numerical calculation, which is related to the complexity of the simulation problem, the quality of the grid, and the value of the relaxation factor in the algorithm.

Therefore, the value of r should be appropriate to take into account the calculation accuracy and convergence, which requires r to be as small as possible under the premise of ensuring accuracy. For this purpose, it is necessary to quantitatively analyze the mathematical relationship between fraction of latent heat, saturation temperature difference, and mass transfer factor r. [47]

Sensible heat exchange：

$$Q_{\mathrm{sen}} = c_{p,m}G(T_{\mathrm{out}} - T_{\mathrm{sat}}) \tag{10}$$

Latent heat exchange：

$$Q_{\mathrm{lat}} = \frac{Har\rho_{\mathrm{l}}h_{\mathrm{fg}}\alpha_{\mathrm{g}}L\Delta T}{2T_{\mathrm{sat}}} \tag{11}$$

Latent heat fraction：

$$R_{\mathrm{L}} = \frac{Q_{\mathrm{lat}}}{Q_{\mathrm{lat}} + Q_{\mathrm{sen}}} \tag{12}$$

Saturation temperature difference：

$$\Delta T = T_{\mathrm{sat}} - T_{\mathrm{out}} \tag{13}$$

$$\Delta T = \frac{aLq}{C_{p,m}G + (r\rho_{\mathrm{lin}}\alpha_{\mathrm{g}}h_{\mathrm{fg}}LHa)/2T_{\mathrm{sat}}} \tag{14}$$

According to the energy equation, the value of r determines the proportion of latent heat transfer to the total heat transfer. As proposed by Qiu et al. [47], single-component boiling heat transfer is generally considered constant-pressure phase-change heat transfer, where the temperature variation of the fluid in the two-phase region is minimal, and heat transfer is dominated by phase change, with the latent heat fraction (R_L) expected to approach 1.

In this study, when $r \geq 600$, numerical instability and divergence of the equations began to occur. When r was set to 500, the variation rate of R_L was 1.1%, and $|\Delta T| < 1$°C, satisfying the assumptions. Therefore, in all subsequent cases, r was fixed at 500 to ensure the stability and accuracy of the energy equation solution.

Tab. 1 Equation calculation and simulation verification for the value of r.

r	R_L		$\|\Delta T\|$ /°C	
	Ref. [38]	this work	Ref. [38]	this work
100	1	0.896	2.64×10^{-2}	5.59
300	1	0.972	3.25×10^{-3}	1.40
500	1	0.983	1.73×10^{-3}	0.88
600	1	divergence	1.44×10^{-3}	divergence

2.3. Boundary conditions and numerical methods

The inlet boundary conditions are constant velocity and constant temperature as follows.

$$v = v_{in}, T = T_{sat}, x_{in} = C, \alpha_v = C \tag{15}$$

The outlet boundary condition is constant pressure as follows.

$$P = P_{sat} \tag{16}$$

For the heat wall of the heat sink, the constant wall heat flux boundary condition is adopted.

$$q = q_s \tag{17}$$

In this work, numerical simulation was performed using ANSYS FLUENT 23.1, a commercial program for fluid dynamics computation. The pressure-velocity coupling was resolved using the Coupled algorithm, and the Modified Body Force Weighted scheme was used to solve the pressure equation. Discretization of the momentum and energy equations was performed using a second-order upwind scheme. For the continuity equation, momentum equation, and energy equation, the normalized residuals have to be smaller than 10^{-4}, 10^{-6}, and 10^{-8} for the computational solutions to be deemed convergent.

The simulated refrigeration cycle conditions are evaporation temperature of -25°C, condensation temperature of 53.6°C, subcooling degree of 5°C, superheat degree of 5°C, inlet refrigerant quality of 0.48, and wall heating capacity satisfying a cooling capacity of 120W. As indicated in Tab. 2, the study investigates both positive and negative inclinations ranging from 0° to 90° under variable inclination conditions, while maintaining a constant inlet flow rate, for three structural aspect ratios (a, b, c). Additionally, for variable inlet Reynolds number conditions, the inlet velocity is adjusted to achieve $\Delta Re = 500$.

Tab. 2 Numerical simulation working conditions.

Geometry Type	Angles [°]	Inlet Velocity [m/s]
a、b、c	0	5.99
	15, -15	5.99
	30, -30	5.99
	45, -45	5.99
	60, -60	5.99
	75, -75	5.99
	90, -90	5.99
a	15	5.99
	15	5.31
	15	4.55
	15	3.79
	15	3.03

2.4. Grid independence verification

Fig. 3 depicts the average wall temperature (°C) on the left y-axis and the pressure difference between the inlet and outlet (Pa) on the right y-axis. When the number of grids increased to 1.95 million, the calculation results did not change much within 0.32%. Therefore, considering the required accuracy and computational cost, 196 million grids were finally selected for numerical simulation.

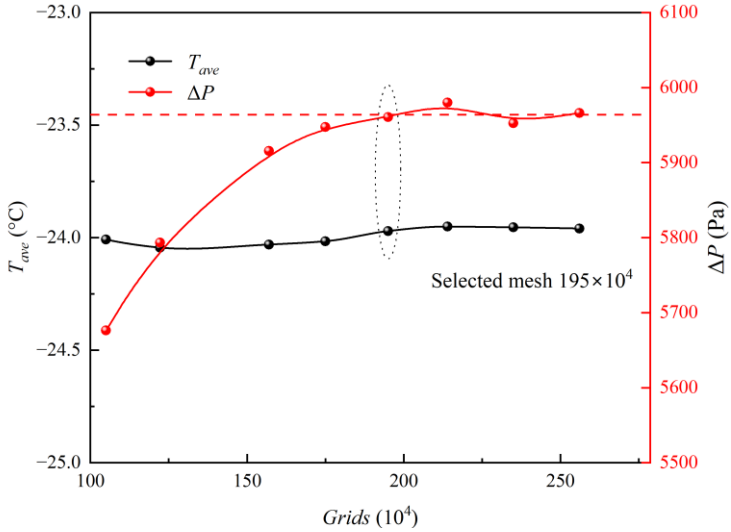

Fig. 3. Grid convergence: T_{ave} and ΔP (type b, Re=3946).

3. Pressure drop and heat transfer coefficient in flow boiling

In order to verify the accuracy of the model, the temperature change along the path of the same simulated tube was tested under the condition of 15° inclination. The experimental tests were performed on a freezer with a rated cooling capacity of 120W. The heat exchange tube of the evaporator was a micro-channel flat tube measuring 6.5 metres in length. The Pt1000 thermocouples were evenly placed on the wall far from the inner tank, wrapped with aluminum foil tape and fixed. The evaporator's inlet and outlet were fitted with pressure sensors. During steady-state operation, the temperature distribution on the wall surface of the micro-channel flat tube is shown in Fig. 4.

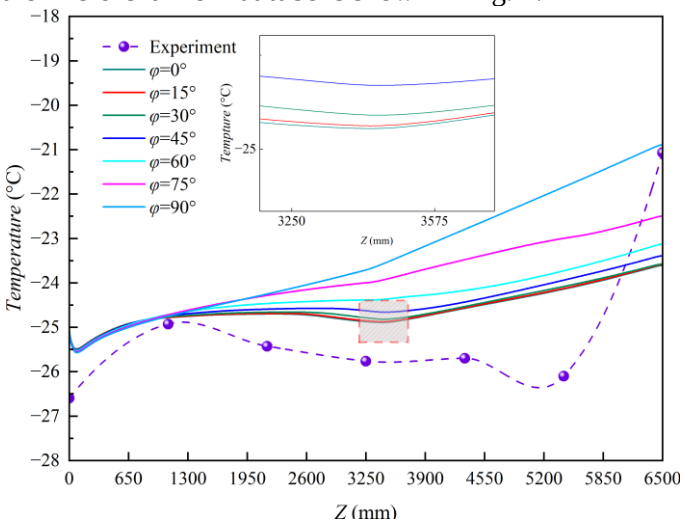

Fig. 4. Iso-wall temperature: simulation vs experiment (type a).

In the range of inclination angles from 0° to 45°, the simulated data is consistent with the experimental temperature trends. When Z was greater than 5200 mm, the measured temperature increased significantly, and the degree of superheat reached 4 °C. Analysis indicates that the freezer box structure, hot air infiltration from the top cover, and uneven temperature distribution contributed to the use of the lower inlet-outlet scheme, resulting in accelerated drying and superheat of the refrigerant in the microchannel flat tube near the exit.

In the simulation, the flow of refrigerant in the second half of boiling was kept stable by using a constant wall heat flux. The maximum temperature error at Z = 5416 mm was 1.972°C, and the inlet and outlet pressure simulation results deviated from the experimental results by 24.9%. Considering the pressure loss due to the microchannel flat tube wrapped around the inner liner surface, the steady-state simulation model is reliable.

3.1. Pressure drop variation

Fig. 5 depicts the difference in pressure drop ($\Delta(\Delta P) = \Delta P_+ - \Delta P_-$) between the inlet and outlet for both forward (ΔP_+) and reverse (ΔP_-) directions at the same inclination angle on the left y-axis, while the rate of change in pressure difference ($\Delta(\Delta P)/\Delta P_-$) for the same conditions is shown on the right y-axis. The difference in pressure drop on the left y-axis shows significant variations between positive and negative directions, while the rate of change in pressure difference on the right y-axis reveals the corresponding dynamic characteristics. The variation of refrigerant pressure in the tube under 7 inclination angles ranging from 0° to 90° was simulated and compared. The influence of different inclination angles of the heat exchange tube and the inlet/outlet configuration on the inlet/outlet pressure difference of the chest freezer evaporator has been obtained. Each bar chart represents the difference in ΔP under different inlet modes. For angles of 15° and 30°, using the upper inlet and lower outlet configuration reduced the pressure drop by 29.1 Pa and 54.7 Pa, respectively, compared to the lower inlet and upper outlet configuration, with reduction rates of 0.48% and 0.92%. For angles of 45°, 60°, 75°, and 90°, using the upper inlet and outlet configuration reduced the pressure drop by 80 Pa, 98.2 Pa, 110 Pa, and 114 Pa, respectively, with reduction rates of 1.35%, 1.67%, 1.89%, and 1.97%.

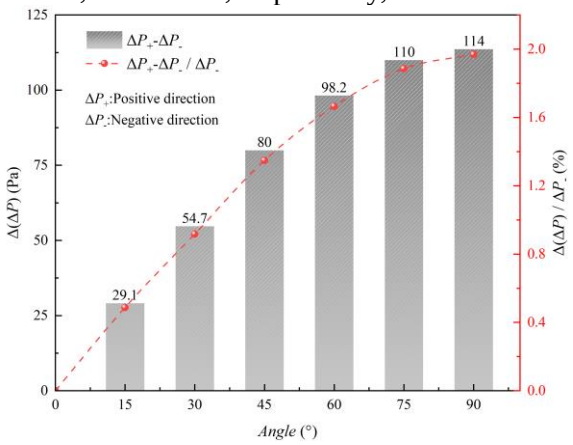

Fig. 5. Pressure divergence of type a between dual inlet modes.

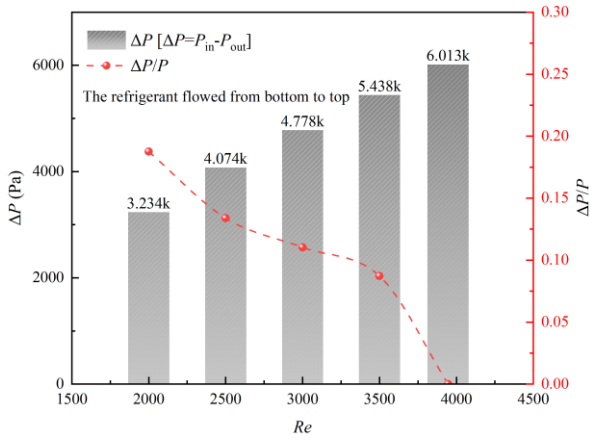

Fig. 6. Simulated ΔP and scaled $\Delta P/P$ versus *Re*.

In the evaporator micro-channel heat exchange tube used in the chest freezer, the configuration scheme of refrigerant flow from top to bottom can effectively reduce the pressure drop. When the inclination angle exceeds 60°, the rate of pressure drop decreases significantly, and the ratio $\Delta(\Delta P/P)$ tends to stabilize. $\Delta(\Delta P/P)$ indicates the change rate of pressure drop relative to total pressure. When stable, further inclination results in less significant pressure drop reduction. For chest freezer evaporator tubes, top-to-bottom refrigerant flow reduces pressure drop notably up to 60° inclination. Beyond this, the effect diminishes. Thus, design should balance pressure drop reduction, heat exchange efficiency, and manufacturing cost to find the best inclination and configuration.

Currently, research on flow boiling in microchannels has primarily emphasized the management of high heat flux density and high mass flow rate in hot spots. Nevertheless, little attention has been paid to studying low *Re* conditions at the microchannel evaporator inlet in small, low-mass flow horizontal freezers. In this work, the pressure drop effect of 6500 mm long length-to-diameter ratio a-type microchannel flat tube with an inclination of 15° was studied. The refrigerant flowed from bottom to top, and the inlet Reynolds number ranging from 2000 to 4000, and the simulation was conducted using a laminar flow model. The variations in pressure drop between inlet and outlet simulated by laminar flow models in the range of 2000-4000 Reynolds numbers were shown in Fig. 6. As the inlet Reynolds number decreases, the pressure drop to total pressure ratio ($\Delta P/P$) gradually increased to 0.187. It was worth noting that when the *Re* number approaches the transition region between laminar flow and

turbulence, the change rate of $\Delta P/P$ was significantly higher than the value when the *Re* number is 2500 ~ 3500.

3.2. Heat transfer coefficient of flow boiling at different inclinations

As illustrated in Fig. 7, the convection HTC along the refrigerant flow direction distribution is nearly the same under conditions of the same inclination angle, with the refrigerant flowing down into and out of the two ways and a constant heat flux density of 416 W/m². This is due to, on one hand, the simulation of the state of refrigerant inlet to the evaporator for the gas-liquid two-phase and the refrigerant gas volume fraction in the low-dry condition (quality = 0.48). When R600a is used as a refrigerant, the volume fraction of refrigerant gas remains above 99% at low dryness, the refrigerant gas occupies most of the flow space, and the refrigerant liquid flows forward under the coercion of the refrigerant gas. On the other hand, due to the high refrigerant center flow rate inside the tube, the influence of gravity on the refrigerant flow rate inside the tube is not obvious. The pressure difference between the inlet and outlet ends of the evaporator under positive and negative inclination is mainly influenced by the potential pressure.

Under different inclinations, the wall convection HTC fluctuates twice along the flow direction at *Z*=650mm and *Z*=3250mm, respectively, as shown in Fig. 7 and Fig. 8. At 0° inclination, refrigerant liquid volume fraction trends align with wall convection HTC fluctuations at X=0.13628. As shown in Fig. 7, in type a, the smaller the inclination, the more obvious the two fluctuations occur, and the peak appears earlier. With the inclination increases, the second fluctuation of the wall convection HTC occurs further back in the flow direction. Specifically, the convection HTC is significantly higher on average at inclination angles of ±75° compared to other inclination conditions.

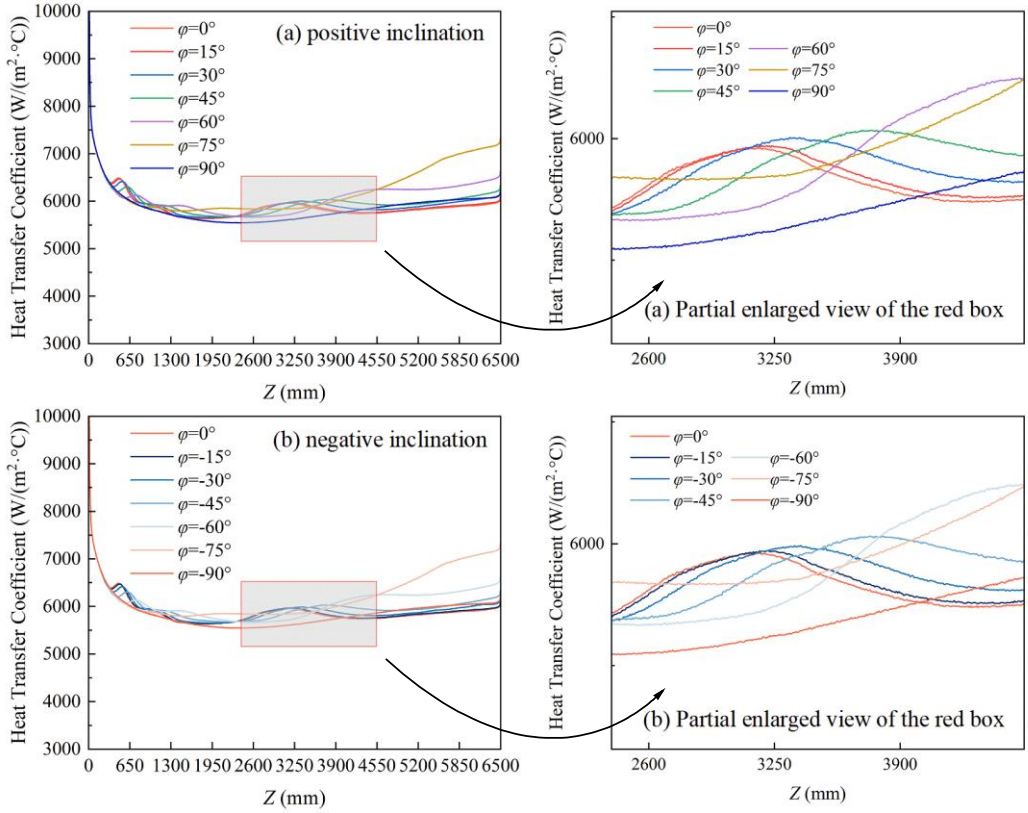

Fig. 7. Variation of flow boiling HTC at different inclinations (type a, q=416 W/m²):(a) positive inclination with partial enlarged view (b) negative inclination with partial enlarged view.

To study the relationship between the inclination angle and the convective HTC during the boiling of microchannel flow with various aspect ratio constructions, the changes of the convective HTCs along the inclination angle of the two β structures (type b, type c) under the same boundary conditions are shown in Fig. 2. Combined with Fig. 8, Fig. 9(a), it is discovered that the fluctuation of the along-stream convective HTC at the inlet section Z=650 mm gradually decreases as β decreases by 20%, and the fluctuation at Z=650 mm almost disappears when β is 0.763. The simulation results from the two

different inlet modes show no significant difference in the magnitude of the wall convection HTC. Therefore, for three different β, the lower inlet and upper outlet mode is adopted as an example, as only the inlet and outlet pressure drop exhibits a significant difference. When β is reduced by 20%, at the 0° inclination, the convective HTC of type b compared to type c decreases by 11.1%. For various other inclinations, the convective HTC of fluid-solid coupled wall shows a significant decreasing trend, with a 16.6% and 11.6% average decline, respectively. According to Andredaki et al. [53], as the aspect ratio decreases, the dominant heat transfer mechanism shifts from contact line evaporation to liquid film evaporation. The aspect ratio of the microchannel significantly influences local heat transfer characteristics, leading to a decrease in the HTC. This is due to changes in bubble growth dynamics during two-phase flow development, which result in a dynamic redistribution of contributions between contact line evaporation and liquid film evaporation. Within the range of 0-75° inclination, the average convective HTC of the type a wall increases by an average of 1.096% for every 15° increase in inclination. The average convective HTC of the wall of type b increased by 5.353% per 15° with the increase of inclination in the range of 0-60°. In the 0-90° range, as the inclination increases, the type c wall average convective HTC per 15° average decline is 3.618%. Therefore, when using the bottom-in, top-out method and heating the microchannel flat tube on one side against the wall, microchannel structures with β less than 1 should be avoided to enhance the heat transfer effect at the fluid-solid coupling interface across multiple inclinations.

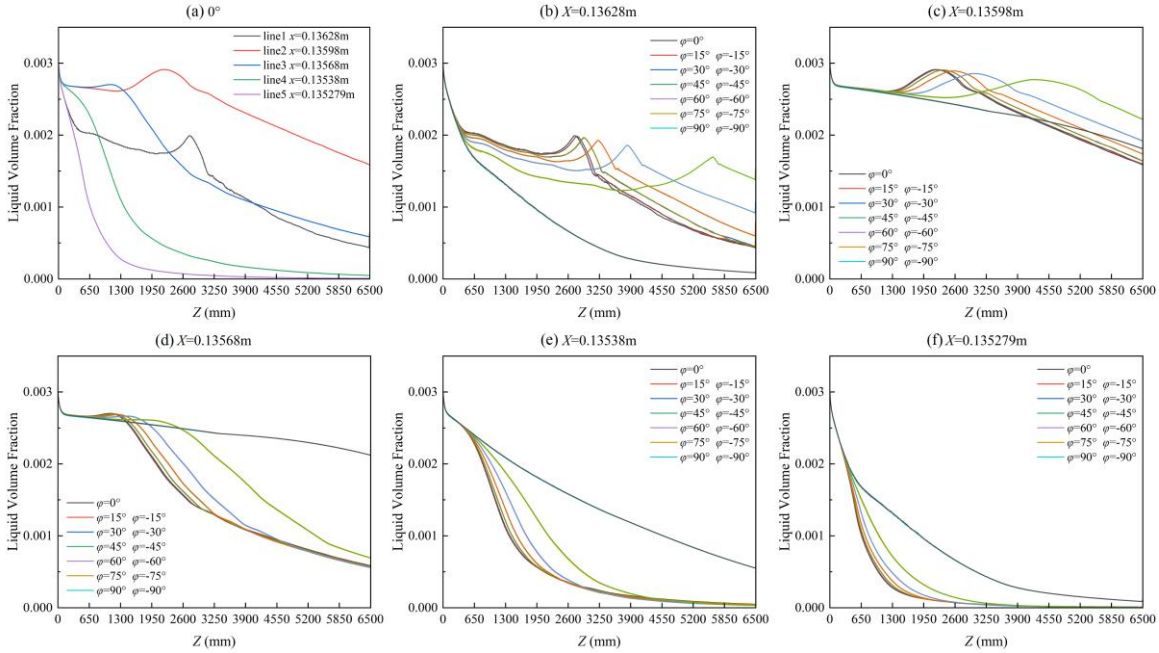

Fig. 8. LVF variation of A at width center along height:(a) 0° (b) X=0.13628m (c) X=0.13598m (d) X=0.13568m (e) X=0.13538m (f) X=0.135279m.

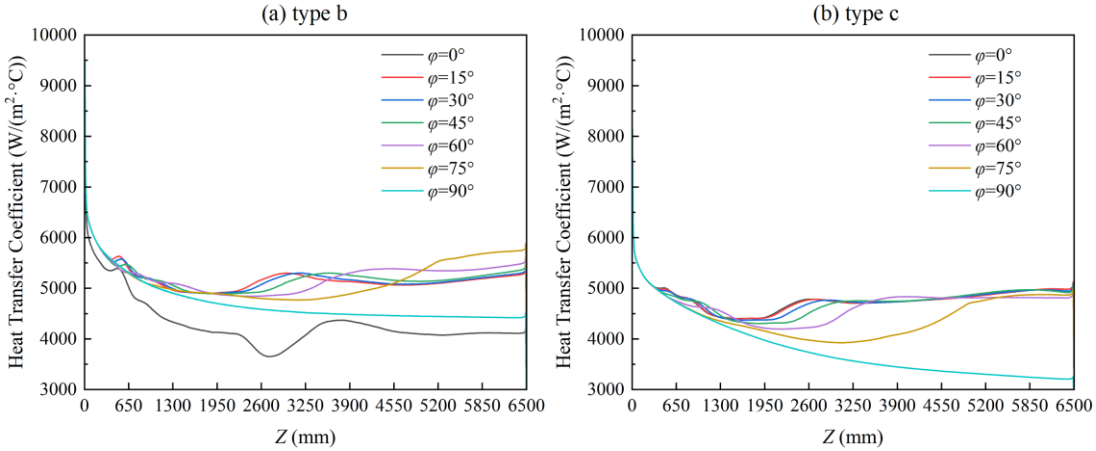

Fig. 9. Variation of HTC along the flow path:(a) type b (b) type c.

3.3. Liquid Volume Fraction and Heat Transfer Coefficient under different *Re*

Along the length of the tube, the Reynolds number significantly affects the refrigerant's temperature distribution. When the mass flow rises, the volume of vapor slugs reaching the outlet of the micro-channel decreases.[53]. As shown in Fig. 10, as the microchannel evaporator inlet refrigerant *Re* number decreases, in the adiabatic wall surface at the center of the temperature, the position of superheat gradually moves forward; from Z = 3250 mm, it gradually advances to Z = 1950 mm. The evaporator outlet superheat gradually increased from 1°C to more than 10°C.

The temperature curve at all the *Re* numbers of the adiabatic wall surface monitoring point temperature curve shows that the inlet first drops and then quickly backs up the temperature to maintain. As the *Re* number of the inlet refrigerant decreases, the faster the rate of increase of the outlet refrigerant superheat increases. At all tested Reynolds numbers, the temperature profiles recorded at the adiabatic wall monitoring points consistently exhibited a distinct pattern: an initial temperature decrease at the inlet region, followed by a rapid recovery. After reaching a transient steady state, the temperature subsequently exhibited a persistent upward trend, culminating in an overheating phenomenon. With the evaporation of the refrigerant in the tube in the second half of the curve, the surface temperature of the adiabatic wall starts to rise gradually, and the superheating phenomenon is obvious. This phenomenon can be attributed to the increased velocity of the generated bubble, which consequently reduces the time available for evaporation.

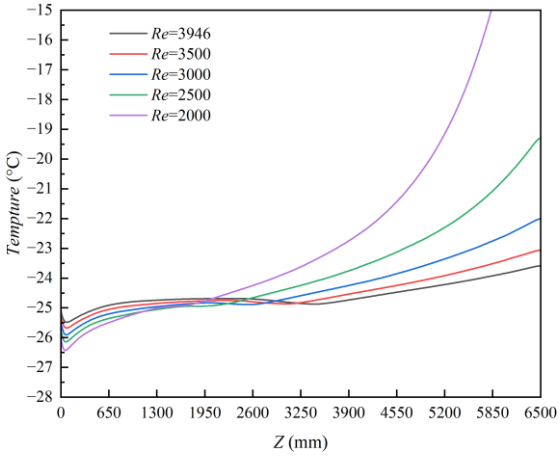

Fig. 10. T_{iso} of Structure A (φ=15°) vs *Re*.

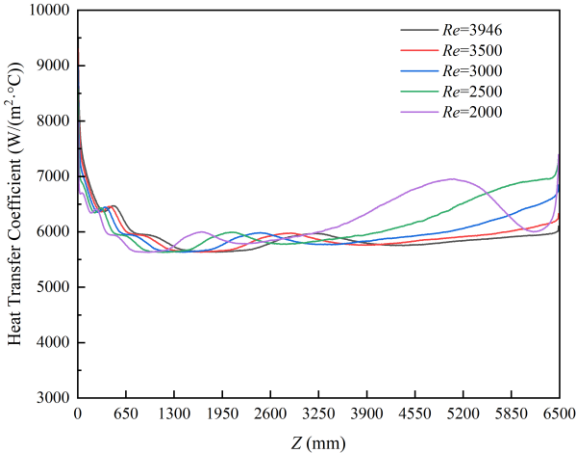

Fig. 11. HTC of Structure A at φ=15° vs *Re*.

Within the range of Z = 0mm to Z = 1300mm, on the microchannel flat tube evaporator's inner wall, the convection HTC is greatly impacted by the entrance section. It steadily declines in the refrigerant flow direction.

Subsequently, as the flow pattern stabilises, the refrigerant inside the flat tube is gradually deposited by gravity in the direction of gravity. In a horizontal orientation, the temperature differential between the refrigerant's inner wall and adiabatic wall diminishes. The wall convection HTC exhibits a brief peak, as refrigerant evaporates horizontally along the wall and the refrigerant liquid volume fraction gradually decreases in the gravity direction.

A stable air film forms inside the flat tube's wall. In the second half of the tube (Z = 3250mm to Z = 6500mm), as refrigerant evaporation is sufficient and the refrigerant flow rate increases. The temperature difference between the adiabatic wall monitoring point and the wall side, covered by the air film, further decreases, resulting in a further increase in the convection HTC.

To analyze the peak values of adiabatic wall temperature and wall convection HTC at various locations in Fig.11 and Fig.12, six points were selected along the gravity direction centered on the inlet cross-section's X-axis. These points were used to investigate changes in refrigerant liquid volume fraction at different locations during the boiling process along the Z-axis, under varying inlet *Re* numbers. Taking the inlet *Re* of 3946 as an example, the refrigerant liquid completes its redistribution within the range of Z=650mm to 1500mm due to gravity. The completion of this redistribution shifts backward along the gravity direction.

Following redistribution, the refrigerant liquid volume fraction decreases slowly along the Z-axis, with a gradually diminishing rate of decrease. This is attributed to the acceleration of the refrigerant in

the tube, influenced by the evaporator inlet and outlet pressure difference, which shortens the wall heating time in the second half of the heat exchanger, enhancing convective heat transfer.

As the inlet *Re* decreases, the refrigerant liquid vapor dry position in the microchannel evaporator flat tube gradually shifts to the Z-axis's left side. Consequently, the inflection point of the refrigerant liquid volume fraction occurs earlier. The evaporator outlet dryness increases with decreasing inlet *Re*. At the outlet points Y = 0.0405402m to Y = 0.011402m, the maximum differences in refrigerant liquid volume fraction under different inlet *Re* numbers are 3.44×10^{-4}, 7.40×10^{-4}, respectively.

For example, at the monitoring point Y = 0.0406402m near the center of gravity direction, as the inlet *Re* increases from small to large, the location where the refrigerant liquid volume fraction reaches 0.001 differs by 604 mm, 605 mm, 617 mm, and 546 mm, respectively. The outlet refrigerant liquid volume fraction decreases by 26.0%, 44.4%, 71.0%, and 96.3% as the inlet *Re* decreases from large to small.

By analysing the effects of different inlet *Re* of microchannel flat tubes on the refrigerant gas-liquid two-phase distribution, convective HTC magnitude, adiabatic wall temperature inside the tubes at specific inclination angles, and wall heat flow density. Considering the current horizontal freezer refrigeration system, the refrigerant charge is small, the refrigeration system is simple, the evaporator arrangement is limited, and the compressor cost and other considerations, the micro-channel evaporator flat tube inlet refrigerant *Re* number should not be lower than 3000 to ensure that the uniformity of the internal temperature of the freezer case and the outlet superheat is maintained within 5°C.

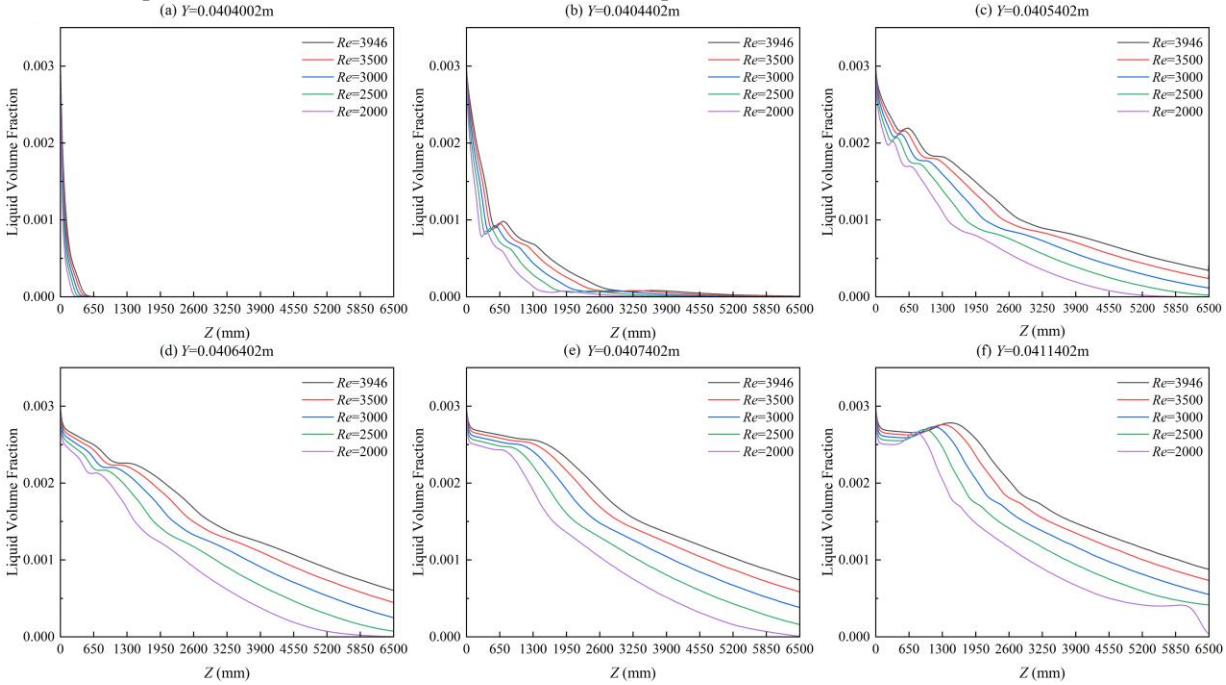

Fig. 12. LVF variation of structure A at width center along height versus *Re*: (a) Y=0.0404002m (b) Y=0.0404402m (c) Y=0.0405402m (d) Y=0.0406402m (e) Y=0.0407402m (f) Y=0.0411402m.

4. Conclusions

To address the challenges of selecting and arranging microchannel heat exchangers during the design phase of refrigerators, a steady-state numerical simulation of flow boiling within a large length-diameter ratio microchannel evaporator was conducted. Using the distributed parameter method in conjunction with the steady-state analysis model of the LEE model [47]. Based on the simulation results, the analysis was performed to assess the consistency between the simulation data and experimental data under the laminar flow model, as well as the influence of varying inclination angles and inlet Reynolds numbers (*Re*) on heat transfer. Adjusting tube geometry and inclination angle in spiral freezer evaporators enhances microchannel heat transfer, reducing pressure drop and maintaining proper superheat to improve system energy efficiency. The detailed results and conclusions obtained are as follows.

(1) Analysis of the convective HTCs for the three structural wall surfaces of a, b, and c at inclination angles of 0-90° (aspect ratios of 1.271, 1.017, and 0.763) revealed a decrease of 16.64% and 11.56% in HTC with decreasing aspect ratio at various inclination angles.

(2) Considering current design requirements for small horizontal freezers with low filling capacity, the use of microchannel flat tubes with an aspect ratio less than 1 should be avoided to maintain uniform internal box temperature.

(3) To ensure that the superheat of the evaporator outlet wall in the existing refrigeration system is controlled within 5°C, the impact of inlet Reynolds number (*Re*) on pressure drop and convective HTC of tube type a was studied in the range of *Re*=2000-3946. The results indicate that the inlet *Re* should not be lower than 3000.

5. Acknowledgments

We are deeply grateful to Dr. Wang, Dr. Song and Dr. Zhou for their invaluable contributions to grammar refinement and theoretical guidance throughout this project. Their meticulous attention to linguistic precision and conceptual clarity significantly enhanced the quality of this work.

We extend special thanks to Mr. Liu for his exceptional project support, which was instrumental in facilitating the successful completion of this research. His organizational expertise and resource coordination created an optimal environment for our team's progress.

6. Disclosure statement

No potential conflict of interest was reported by the author(s).

7. Funding

This work was supported by College Youth Innovation Team of Shandong Province, China (Grant No. 2024KJH151), Young Talent of Lifting Engineering for Science and Technology in Shandong, China (Grant No. SDAST2024QTA048) and Key R & D Program of Shandong Province, China (2022CXGC020901).

8. References

[1] Jiang, X., *et al*., Design of micro-nano structures for counter flow diverging microchannel heat sink with extraordinarily high energy efficiency, *Appl. Therm. Eng*. 209 (2022) 118229.

[2] Ates, A., *et al*., Flow boiling of dielectric fluid HFE–7000 in a minichannel with pin fin structured surfaces, *Appl. Therm. Eng*. 223 (2023) 120045.

[3] Van Erp, R., *et al*., Co-designing electronics with microfluidics for more sustainable cooling, *Nature*. 585 (2020) 211–216.

[4] Priy, A., *et al*., Bubble interaction and heat transfer characteristics of microchannel flow boiling with single and multiple cavities. *J. Therm. Sci. Eng. Appl.* 16 (2024) 061010.

[5] Li, Y., *et al*., Experimental investigation of flow boiling performance in microchannels with and without triangular cavities–A comparative study, *Int. J. Heat Mass Transf*. 108 (2017) 1511–1526.

[6] Kakati, A., *et al*., Influence of the presence of different signatures on the heat transfer profile of laminar flow inside a microchannel. *J. Therm. Sci. Eng. Appl*. 16 (2024) 101002.

[7] Liang, X., *et al*., Manipulation of droplets and bubbles for thermal applications, *Droplet*. 1 (2022) 80–91.

[8] Ma, X., *et al*., Flow boiling heat transfer characteristics on micro-pin-finned surfaces in a horizontal narrow microchannel. *Int. J. Heat Mass Transf*. 194 (2022) 123071.

[9] Ma, X., *et al*., Flow boiling instability and pressure drop characteristics based on micro-pin-finned surfaces in a microchannel heat sink. *Int. J. Heat Mass Transf*. 195 (2022) 123168.

[10] Yang, F., *et al*., Single-and two-phase thermal transport in microchannels with embedded staggered herringbone mixers, *J. Microelectromech. Syst*. 23 (2014) 1346–1358.

[11] Datta, A., *et al*., The role of flow structures on the thermal performance of microchannels with wall features. *J. Therm. Sci. Eng. Appl*. 13 (2021) 021019.

[12] Li, Y., Wu, H., Experiment investigation on flow boiling heat transfer in a bidirectional counter-flow microchannel heat sink, *Int. J. Heat Mass Transf*. 187 (2022) 122500.

[13] Hung, T.C., *et al*., Analysis of heat transfer characteristics of double-layered microchannel heat sink, *Int. J. Heat Mass Transfer*. 55 (2012) 3090–3099.

[14] Hung, T.C., Yan, W.M., Enhancement of thermal performance in double-layered microchannel heat sink with nanofluids, *Int. J. Heat Mass Transfer*. 55 (2012) 3225–3238.

[15] Soleimani, A., *et al*., Thermal analysis of a microchannel heat sink cooled by two-phase flow boiling of al2o3 hfe-7100 nanofluid, *Therm. Sci. Eng. Prog*. 20 (2020) 100693.

[16] Dai, X., *et al*., Enhanced single-and two-phase transport phenomena using flow separation in a microgap with copper woven mesh coatings, *Appl. Therm. Eng*. 54 (2013) 281–288.

[17] Han, Q., *et al*., Enhanced thermal performance by spatial chaotic mixing in a saw-like microchannel, *Int. J. Therm. Sci*. 186 (2023) 108148.

[18] Li, W., *et al*., Experimental and theoretical studies of critical heat flux of flow boiling in microchannels with microbubble-excited high-frequency two-phase oscillations, *Int. J. Heat Mass Transf*. 88 (2015) 368–378.

[19] Morshed, A., *et al*., Enhanced flow boiling in a microchannel with integration of nanowires, *Appl. Therm. Eng*. 32 (2012) 68–75.

[20] Tan, K., *et al*., Enhancement of flow boiling in the microchannel with a bionic gradient wetting surface, *Appl. Therm. Eng*. 230 (2023) 120784.

[21] Eltaweel, A., Hassan, I., A multivariable numerical investigation of wavy-based microchannel heat sink geometry toward optimal thermal performance. *J. Therm. Sci. Eng. Appl*. 16 (2024) 111008

[22] Prajapati, Y.K., *et al*., Numerical investigation of subcooled flow boiling in segmented finned microchannels, *Int. Commun. Heat Mass Transf*. 86 (2017) 215–221.

[23] Zu, Y.Q., *et al*., Confined bubble growth during flow boiling in a mini−/micro-channel of rectangular cross-section part II: approximate 3-D numerical simulation, *Int. J. Therm. Sci*. 50 (3) (2011) 267–273.

[24] Pi, S., *et al*., Numerical investigation of thermal performance of key components of electric vehicles using nucleate boiling, *J. Therm. Sci. Eng. Appl*. 13 (6) (2021) 061021–061027.

[25] Y. C. Liu, *et al*., Study on pressure drop characteristics of multiangle gravity separated heat pipe evaporator. *Scientific and Technological Innovation* (12) (2020) 39-40.

[26] Y. C., Liu, *et al*., Effect of inclination angle on performance of annular heat pipe evaporator. *J. Therm. Sci. Technol*. 20 (06) (2021) 537-546.

[27] S. Saisorn, *et al*., The difference in flow pattern, heat transfer and pressure drop characteristics of mini-channel flow boiling in horizontal and vertical orientations. *Int. J. Multiphase Flow*. 101 (2018) 97-112.

[28] Oliveira, *et al*., An experimental investigation on flow boiling heat transfer of R-600a in a horizontal small tube. *Int J Refrig*. 72 (2016) 97-110.

[29] Ghajar, A.J., Tang, C.C., Heat transfer measurements, flow pattern maps, and flow visualization for non-boiling two-phase flow in horizontal and slightly inclined pipe. *Heat Transf. Eng*. 28(6) (2007) 525-540.

[30] Li, W., *et al*., Experimental and theoretical studies of critical heat flux of flow boiling in microchannels with microbubble-excited high-frequency two-phase oscillations, *Int. J. Heat Mass Transf*. 88 (2015) 368–378.

[31] Qu, W., Mudawar, I., Measurement and correlation of critical heat flux in two-phase micro-channel heat sinks, *Int. J. Heat Mass Transf*. 47 (2004) 2045–2059.

[32] Cui, P., Liu, Z., Experimental study on flow boiling in ultrahigh-aspect-ratio copper microchannel heat sink, *Appl. Therm. Eng*. 223 (2023) 119975.

[33] Wang, Y., *et al*., Flow boiling in high-aspect ratio mini-and micro-channels with FC-72 and ethanol: Experimental results and heat transfer correlation assessments, *Exp. Therm Fluid Sci*. 36 (2012) 93–106.

[34] Lee, W.H., A Pressure Iteration Scheme for Two-Phase Flow Modeling. (2002).

[35] Kharangate, C.R., Mudawar, I., Review of computational studies on boiling and condensation. *Int J Heat Mass Transf*. 108 (2017) 1164-1196.

[36] Yang, Z., *et al*., Numerical and experimental investigation of two-phase flow during boiling in a coiled tube. *Int J Heat Mass Transf*. 51(5) (2008) 1003-1016.

[37] Bahreini, M., *et al*., Numerical simulation of bubble behavior in subcooled flow boiling under velocity and temperature gradient. *Nucl. Eng. Des*. 293 (2015) 238-248.

[38] Lee, J., *et al*., 3-D computational investigation and experimental validation of effect of shear-lift on two-phase flow and heat transfer characteristics of highly subcooled flow boiling in vertical upflow. *Int J Heat Mass Transf*. 150 (2020) 119291.1-119291.19.

[39] Devahdhanush, V.S., *et al*., Assessing advantages and disadvantages of macro- and micro-channel flow boiling for high-heat-flux thermal management using computational and theoretical/empirical methods. *Int J Heat Mass Transf*. 169 (2021) 120787.1-120787.25.

[40] Hasanpour, B., *et al*., Numerical investigation of saturated upward flow boiling of water in a vertical tube using VOF model: effect of different boundary conditions. *Heat and Mass Transfer*. 54 (2018) 1925-1936.

[41] Hedau, G., *et al*., Experimental and numerical investigation of the effect of number of parallel microchannels on flow boiling heat transfer. *Int J Heat Mass Transf*. 158 (2020) 119973.1-119973.18.

[42] Huang, F., *et al*., Numerical analysis on flow pattern and heat transfer characteristics of flow boiling in the mini-channels. *Numer. heat transf*. 78(4) (2020) 221-247

[43] Bahreini, M., *et al*., Numerical simulation of subcooled flow boiling under conjugate heat transfer and microgravity condition in a vertical mini-channel. *Appl. Therm. Eng*. 113 (2017) 170-185.

[44] Lorenzini, D., Joshi, Y.K., Computational fluid dynamics modeling of flow boiling in microchannels with nonuniform heat flux. *J Heat Transfer*. 140(1) (2018) 011501.1-011501.11.

[45] Yeo, I., Lee, S., 2D computational investigation into transport phenomena of subcooled and saturated flow boiling in large length to diameter ratio micro-channel heat sinks. *Int J Heat Mass Transf*. 183 (2022) 122128.1-122128.23.

[46] Dong, F., *et al*., A novel interphase mass transfer model toward the VOF simulation of sub-cooled flow boiling. *NUMER HEAT TR A-APPL*. 76(4) (2019) 1-12.

[47] Qiu, G.D., et al, Analysis on the value of coefficient of mass transfer with phase change in Lee's equation. *Journal of the Harbin Institute of Technology*. (2014) n.pag.

[48] Hirt, C.W., Nichols, B.D., Volume of fluid (VOF) method for the dynamics of free boundaries, *J. Comput. Phys*. 39 (1) (1981) 201–225

[49] Rajalingam, A., Shubhankar, C., Fluid flow and heat transfer characteristics of a microstructured microchannel heat sink under flow boiling condition, *Appl. Therm. Eng*. 248 (2024) 123265.

[50] Pan, L., *et al*., Experimental study on the flow boiling pressure drop characteristics in parallel multiple microchannels, *Int. J. Heat Mass Transf*. 116 (2018) 642–654.

[51] Lorenzini, D., Joshi, Y., Effect of surface wettability on flow boiling in a microchannel, in: Proceedings of CHT-15. 6th International Symposium on Advances In Computational Heat Transf Res, 2015.

[52] Lee, W.H., Pressure iteration scheme for two-phase flow modeling, In" *Multiphase transport: fundamentals, reactor safety, applications*". (1980) 407–432.

[53] Andredaki, M., *et al*., The effect of channel aspect ratio on flow boiling characteristics within rectangular micro-passages. *Int. J. Heat Mass Transf*. 183 (2022) 122201.

Submitted: 06.4.2025.
Revised: 24.6.2025.
Accepted: 09.7.2025.